Article

Influence of Resins on the Structure and Dynamics of SBR Compounds: A Solid-State NMR Study

Michele Pierigé [1], Francesca Nerli [1], Francesca Nardelli [1,2,*], Lucia Calucci [2,3], Mattia Cettolin [4], Luca Giannini [4], Marco Geppi [1,2,3,*] and Francesca Martini [1,2,3]

1   Dipartimento di Chimica e Chimica Industriale, Università di Pisa, 56124 Pisa, Italy
2   Istituto di Chimica dei Composti Organo Metallici, Consiglio Nazionale delle Ricerche, 56124 Pisa, Italy
3   Centro per l'Integrazione della Strumentazione Scientifica dell'Università di Pisa (CISUP), 56126 Pisa, Italy
4   Pirelli Tyre SpA, 20126 Milano, Italy
*   Correspondence: francesca.nardelli@pi.iccom.cnr.it (F.N.); marco.geppi@unipi.it (M.G.)

Abstract: The tackifying effect of resins used in the tire industry highly depends on the compatibility and interaction strength with the rubber matrix. Here, uncured and cured styrene/butadiene rubber compounds, either in the presence or absence of a hydrocarbon aromatic tackifying resin, were studied by means of high-resolution and time-domain solid-state NMR (SSNMR) techniques to investigate resin/polymer interactions and the effect of the resin on the dynamics of polymer chains. ^{13}C direct excitation and cross-polarization spectra, combined with low-field measurements of ^{1}H T_1 and analysis of ^{1}H on-resonance free-induction decay, provided information on the dynamic heterogeneity of the samples and the degree of mixing between the resin and the rubber matrix. Moreover, ^{1}H T_1 and $T_{1\rho}$ relaxation times at variable temperatures were used to investigate the effect of resin on both segmental dynamics activated at the glass transition and collective polymer dynamics. SSNMR findings were discussed in relation to crosslink density and T_g data. The obtained results show that the resin is intimately mixed with the polymer, while maintaining its rigid character. A slowdown of segmental dynamics, related to an increase in T_g, was found as a consequence of resin addition, while no effect was evidenced on fragility and collective polymer dynamics.

Keywords: time-domain NMR; MAS NMR; field-cycling NMR; spin–spin nuclear relaxation; spin–lattice nuclear relaxation; segmental dynamics; polymer dynamics; styrene/butadiene rubber; α-methylstyrene/styrene resin; vulcanization

1. Introduction

Elastomer-based compounds are widely employed in the tire industry thanks to the possibility to tune their applicative properties by modifying their formulation. Usually, they are composed of one or more polymers, such as natural rubber or synthetic polymers (isoprene rubber, butadiene rubber, styrene/butadiene rubber), which are subjected to vulcanization in the presence of a vulcanizing agent and other ingredients, including fillers, stabilizers, processing oils and resins, with the purpose of providing defined mechanical proprieties to the final product [1]. In particular, resins are employed in the tire industry for the following three different functions: as tackifiers; as reinforcing agents; and as curing agents [2]. Specifically, tackifying resins are added to modify the rheological behavior of the rubber compound, with the final aim of favoring the processability of the uncured compound, promoting filler dispersion and improving mechanical properties of tires, such as rolling resistance and wet traction [1–7]. The achievement of precise requirements in the final product strongly depends on the polymer–resin miscibility, which in turn is related to physico-chemical characteristics of the resin itself, such as the softening point, glass transition temperature (T_g), viscosity, chemical structure and molecular weight [6–14]. Indeed, the presence of resin alters the dynamics of the polymer chains, resulting in a modification

of the viscoelastic behavior and final mechanical properties of the vulcanizate [14–16]. In this frame, the comprehension of the relationship between macroscopic proprieties of technological interest and structural and dynamic features arising from polymer–resin interactions at the molecular level plays a key role in rationalizing the design of new materials with improved performances. A common way to evaluate polymer–resin miscibility and to predict the effect of resin on the mechanical behavior of the final product relies on monitoring the T_g of the vulcanizate upon resin addition. This is often conducted either by calorimetric measurements [12,17,18] or by dynamic mechanical analyses [6–11,19]; in the latter case, the tanδ curve as a function of temperature is measured, whose profile is directly influenced by the change in T_g and provides a way to predict the behavior of the vulcanized blend in terms of rolling resistance and wet traction. Other studies investigate the effect of resins on the dynamic [13–15], viscoelastic [16], and mechanical [17,18,20,21] properties of rubbers.

Solid-state NMR spectroscopy (SSNMR) represents a valuable technique to gain insight into the structure and dynamics of polymeric materials [22–26]. In particular, ^{1}H time-domain (TD) SSNMR experiments can be exploited to measure ^{1}H spin–lattice relaxation times in the laboratory frame (T_1) and in the rotating frame ($T_{1\rho}$), as well as ^{1}H spin–spin relaxation times (T_2), which depend on the modulation of ^{1}H-^{1}H dipolar couplings by molecular motions, thus providing information on the dynamics of polymer chains [27–31]. In addition, in the case of multicomponent systems with domain sizes lower than tens of nm (or nm), the T_1's (or $T_{1\rho}$'s) of protons in different dynamic environments tend to be averaged to a single value due to the spin diffusion phenomenon, thus allowing an assessment of the structural homogeneity of a sample. Moreover, one can also benefit from magic angle spinning (MAS), high-power decoupling, and cross-polarization (CP) techniques to obtain high-resolution SSNMR ^{13}C spectra, which yield both structural and dynamic information on each component of the composite [22,24]. Thanks to the wealth of information that can be obtained, SSNMR has been successfully employed to investigate the dynamic and structural properties of elastomer compounds and vulcanizates. However, to the best of our knowledge, it has not previously been employed to characterize the effect of resins on elastomer structure and dynamics.

In this work, TD and high-resolution SSNMR techniques were applied to investigate uncured and cured styrene/butadiene rubber compounds, either in the presence or absence of the tackifying resin Kristalex™ 5140, a low molecular weight (M_n = 1690 g/mol) α-methylstyrene/styrene copolymer characterized by excellent thermal stability, a high softening point (413 K) and a glass transition temperature of 363 K [32]. ^{13}C high-resolution SSNMR spectra and analyses of on-resonance ^{1}H free-induction decays (FIDs) were used to investigate the structural properties and dynamic and structural heterogeneity of the samples. Information on the heterogeneity of the samples was also obtained from ^{1}H T_1 and $T_{1\rho}$. Moreover, ^{1}H T_1 and $T_{1\rho}$ measured at different temperatures and at different magnetic fields were exploited to characterize the dynamics of the polymeric chains on a wide range of motion timescales. In particular, we took advantage of field-cycling (FC) NMR relaxometry to measure ^{1}H T_1 on a wide range of Larmor frequencies (0.01–35 MHz). The NMR results were discussed in comparison with data on crosslink density and glass transition temperature, two macroscopic properties of interest for rubber applications that are usually affected by the addition of resins. This comparison allowed the effect of the resin on the structure and dynamics of the polymer chains in the rubber compound and the corresponding vulcanizate to be correlated with these applicative properties. Moreover, information could be obtained on the degree of mixing between polymer and resin.

2. Materials and Methods

2.1. Samples

All samples were provided by Pirelli Tyre SpA (Milano, Italy). The sample indicated as SBR consists of a blend of styrene/butadiene rubber (39.5% styrene, vinyl content on the dienic portion 38.5%, M_n = 530,000 g/mol, M_w = 750,000 g/mol), treated distilled aromatic

extract (TDAE) as plasticizer oil, carbon black (N100 series, surface area: 158 m^2/g) as a reinforcing filler and a vulcanization package containing sulfur, N-cyclohexyl-2-benzothiazole sulfenamide (CBS), zinc oxide and stearic acid. Sample SBR_k has the same formulation as SBR, but it also contains Kristalex™ 5140 resin (poly(α-methylstyrene-co-styrene), Synthomer, M_n = 1690 g/mol, M_w = 4750 g/mol). vSBR and vSBR_k indicate samples obtained by the vulcanization of SBR and SBR_k, respectively. All compounds were mixed in a 1.5 L internal mixer (Harburg Freudenberger, Hamburg, Germany) in a two-step mixing process. In the first step, all ingredients, except the vulcanization system, were mixed for 200 s, reaching a dumping temperature of approximately 413 K with a rotor speed of 75 rpm. In the second step, the vulcanization system was added, and the compound was finalized by mixing for 120 s at 313 K with a rotor speed of 50 rpm, and the maximum dumping temperature was set at 383 K. vSBR and vSBR_k were vulcanized at 443 K for 10 min.

The composition of the samples is reported in detail in Table 1.

Table 1. Sample composition in phr (parts per hundred rubber).

Component	SBR and vSBR	SBR_k and vSBR_k
Styrene/butadiene rubber	100	100
TDAE	37.5	37.5
Carbon black	45	45
Sulfur	2	2
CBS	4	4
Zinc oxide	3.5	3.5
Stearic acid	2	2
Kristalex™ 5140	0	15

2.2. Differential Scanning Calorimetry and Equilibrium Swelling Experiments

Differential scanning calorimetry (DSC) measurements were carried out with a DSC Mettler-Toledo 820 instrument. Thermal cycles between 183 and 473 K were performed. The cooling/heating rate was 10 K/min. For all samples, T_g was determined as the intersection point of the two tangents to the DSC curve at the endothermic step. The obtained values are reported in Table 2.

Equilibrium swelling experiments were performed in duplicate to determine the crosslink density ($1/M_c$, where M_c is the average molar mass between two adjacent crosslinks) of vSBR_k and vSBR. The samples were weighed and then soaked in toluene for 72 h in the dark. Thereafter, they were dried with absorbent paper and quickly weighed. After being dried overnight in an oven at 343 K under vacuum, the samples were weighed again in order to determine the amount of adsorbed solvent. $1/M_c$ values were then calculated using the Flory–Rehner equation [33]. The obtained $1/M_c$ values are reported in Table 2.

Table 2. T_g values obtained by DSC experiments and crosslink density ($1/M_c$) values determined by equilibrium swelling experiments.

Sample	T_g (K)	$1/M_c$ (10^{-5} mol/g)
SBR	246	-
SBR_k	249	-
vSBR	253	1.80
vSBR_k	257	1.38

2.3. SSNMR Experiments

^{1}H on-resonance FIDs were recorded at 303 K on a Niumag permanent magnet interfaced with a Stelar PC-NMR console, working at a ^{1}H Larmor frequency of 20.8 MHz and equipped with a single-channel static 5 mm probe. Specifically, the mixed Magic Sandwich Echo (MSE) pulse sequence was applied [23] using a total echo duration $\tau_{MSE} = 6 (4\tau_\varphi + 2\tau_{90})$,

with τ_φ = 1.5 µs and τ_{90} = 3.3 µs. For compounds and vulcanizates, a dwell time of 1 µs was used and 3k data points were acquired. For Kristalex™ 5140, the dwell time was 0.1 µs and 2k data points were acquired. A total of 200 scans were accumulated using a recycle delay of 0.5 s for the compounds and vulcanizates, and one of 1 s for Kristalex™ 5140. The experimental MSE ^{1}H FIDs were analyzed by a discrete approach using a non-linear least-square fitting procedure implemented in the Mathematica$^{\circledR}$ environment [34]. For all samples, ^{1}H longitudinal relaxation time, T_1, values were also measured at 303 K using the inversion recovery pulse sequence coupled with a solid echo pulse scheme (IRSE), with delay times ranging from 1 ms to 0.5 s in the case of the vulcanized samples and from 1 ms to 1 s for Kristalex™ 5140. All IRSE experiments were acquired using 4–16 scans and recycle delays of 0.5 and 1 s for vulcanized samples and Kristalex™ 5140, respectively.

^{13}C high-resolution SSNMR experiments and ^{1}H $T_{1\rho}$ measurements were performed on a Bruker Avance Neo spectrometer working at Larmor frequencies of 500.13 and 125.77 MHz for ^{1}H and ^{13}C nuclei, respectively, using a double-resonance 4 mm CP-MAS probe. 90° pulses with a duration of 4.3 µs and 4.1 µs were employed for ^{1}H and ^{13}C excitation, respectively. ^{13}C direct excitation (DE) spectra under MAS were recorded on vSBR and vSBR_k using a recycle delay of 20 s, optimized to obtain quantitative measurements and accumulating 1600 scans. ^{1}H–^{13}C CP/MAS spectra were recorded on vulcanized samples and on Kristalex™ 5140 by applying a linear ramp on the ^{13}C channel during the contact time, using a constant ^{1}H spin-lock field of 69 kHz. To investigate CP dynamics, contact times ranging from 0.05 to 4 ms were employed for vSBR and vSBR_k, while for Kristalex™ 5140, contact times ranged from 0.05 to 10 ms; 1000 transients were accumulated, using a recycle delay of 4 s. All ^{13}C experiments were recorded at 303 K, applying the SPINAL-64 scheme during acquisition for high-power proton decoupling. An MAS frequency of 5 kHz was used to avoid spinning instability due to the elastic character of the samples. ^{1}H $T_{1\rho}$ measurements were performed at different temperatures between 303 and 343 K and under static conditions by applying a spin-lock field of 46 kHz for durations ranging from 0.4 to 20 ms.

^{1}H longitudinal relaxation rates, $R_1 = 1/T_1$, were measured in a $0.01-35$ MHz Larmor frequency range at different temperatures by means of a Stelar Spin Master FFC-2000 FC NMR relaxometer. The switching time was 3 ms, while the 90° pulse duration was 10.9 µs, and a single scan was acquired. Prepolarized and non-prepolarized pulse sequences were used below and above 12 MHz, respectively. The polarizing and detection frequencies were set at 25 and 16.3 MHz, respectively, while all other parameters were optimized for each experiment. All the ^{1}H magnetization curves vs. time were reproduced using a monoexponential function, with errors on ^{1}H R_1 lower than 3%. Samples were cut into small pieces and loaded in a 10 mm NMR glass tube. Measurements were performed every 10 K from 303 K to 393 K. The sample temperature was controlled within ± 0.1 K by a Stelar VTC90 variable temperature unit. Considering the adopted instrumental conditions, R_1 values higher than 1000 s^{-1} were disregarded.

3. Results and Discussion

3.1. Structural Characterization and Degree of Mixing

The presence of domains with different molecular mobility in the samples was investigated through the analysis of on-resonance ^{1}H FIDs acquired using the MSE pulse sequence [35]. Indeed, this analysis allowed protons in different dynamic environments to be distinguished on the basis of spin–spin relaxation times, ^{1}H T_2, whose values monotonically increase as the degree of mobility increases [35–40].

Figure 1 shows the ^{1}H FIDs obtained for all samples at 303 K. The curves were fitted to a linear combination of three functions (Equation (1)), each characterized by a decay time $T_{2,i}$ and multiplied by a fractional weight W_i ($i = g, e1, e2$) [38,41,42].

$$I(t) = I(0)\left(W_g e^{-\left(\frac{t}{T_{2,g}}\right)^2} + W_{e1} e^{-\frac{t}{T_{2,e1}}} + W_{e2} e^{-\frac{t}{T_{2,e2}}}\right) \quad (1)$$

The first function is a Gaussian function (g), representative of the fraction of protons in rigid environments. The other two are exponential functions ($e1$, $e2$), ascribable to protons in regions of intermediate and fast mobility. An example of FID fitting is shown in the inset of Figure 1, while the best fit values of W_i and $T_{2,i}$ are reported in Table 3.
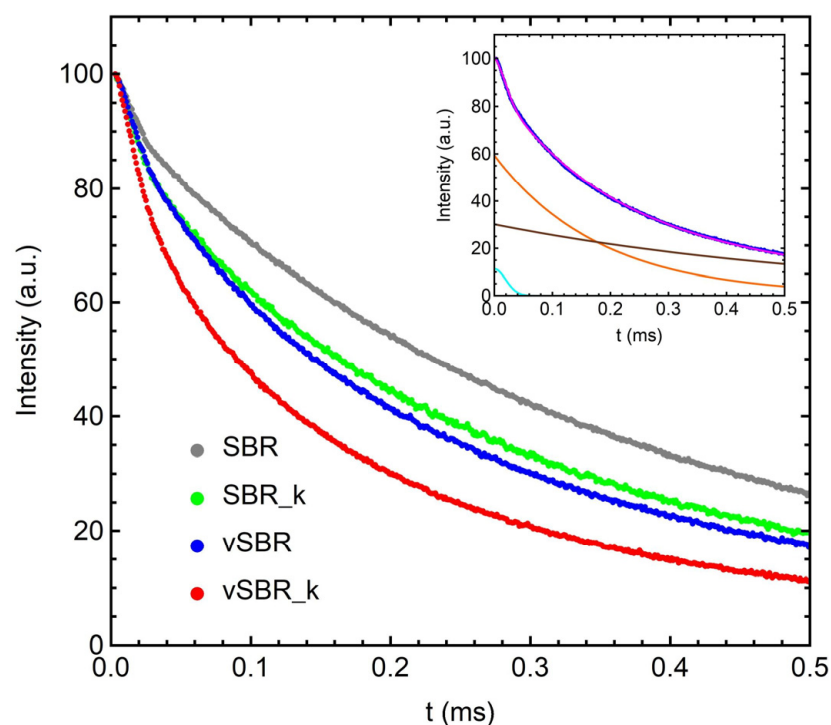
Figure 1. Expansion of the first 0.5 ms of the experimental ^{1}H FIDs of the investigated samples at 303 K. The inset shows the experimental curve (blue) and the total fitting function (magenta) obtained for vSBR, together with the single contributions of the Gaussian (cyan), intermediate-T_2 (orange), and long-T_2 (brown) exponential functions.

Table 3. Weight percentages (W_i) and $T_{2,i}$ values obtained as best-fitting parameters from the analysis of the ^{1}H FIDs of the investigated samples through Equation (1).

Sample	W_g (%)	W_{e1} (%)	W_{e2} (%)	$T_{2,g}$ (µs)	$T_{2,e1}$ (µs)	$T_{2,e2}$ (µs)
SBR	8	65	27	22	296	773
SBR_k	13	56	31	25	216	607
vSBR	11	59	30	27	183	615
vSBR_k	19	57	24	26	139	535

For all the analyzed samples, a small proton fraction associated to the Gaussian function was detected, with a very short T_2 on the order of 20–30 μs, ascribable to molecular fragments with highly restricted mobility, including polymer segments involved in physical and chemical constraints, such as entanglements and crosslinks, and in interactions with filler particles. The two exponential components are instead characterized by longer T_2 values ranging from ~100 to ~800 μs, and they account for most of the protons in the polymer chain segments and for protons in liquid-like components, including TDAE and dangling chains.

By passing from the uncured to the vulcanized samples, an increase in W_g and a concomitant decrease in the T_2 values of both exponential functions were observed. This effect can be ascribed to the formation of chemical crosslinks between the polymer chains, causing a reduction in molecular mobility. As the resin was added, an increase in the rigid fraction on the order of 5–8% was observed, accompanied by a decrease in both $T_{2,e1}$ and $T_{2,e2}$ values. Because the ^{1}H FID of pure resin can be nicely reproduced by a Gaussian function characterized by a T_2 value of 20 μs (Figure S1), the higher W_g values obtained for SBR_k and vSBR_k can reasonably be ascribed to a contribution of the resin protons to the Gaussian component. Indeed, it was estimated that the resin protons account for 10% of the total proton content in both samples. Furthermore, the decrease in $T_{2,e1}$ and $T_{2,e2}$ values reflects a slowdown of the dynamics of all the other components of the samples, mainly the polymer, induced by the presence of resin.

In order to ascribe the regions at different mobilities to different sample components, ^{13}C high-resolution SSNMR experiments were carried out on vSBR and vSBR_k. In particular, ^{13}C DE/MAS spectra were recorded to obtain quantitative spectra, while ^{1}H-^{13}C CP/MAS spectra selectively highlighted the more rigid components of the samples. In fact, the CP process relies on the magnetization transfer from abundant (^{1}H) to rare (^{13}C) nuclei mediated by the heteronuclear dipolar interaction, enhancing the detection of ^{13}C nuclei in close proximity to protons in rigid environments. Furthermore, the CP dynamics is strongly influenced by molecular motions, as they directly affect the extent of dipolar interaction, as well as ^{1}H $T_{1\rho}$, and can be studied by analyzing CP spectra recorded at different contact times.

The ^{13}C DE/MAS spectra acquired for vSBR and vSBR_k are reported in Figure 2a,b. Both spectra presents broad signals, mainly due to the distribution of chemical shifts typical of amorphous materials. Specifically, a group of signals at low chemical shifts (0–50 ppm) is present, ascribable to the aliphatic carbon nuclei of the polymer and TDAE, and to naphthenic carbons in TDAE. In the spectrum of vSBR_k, an additional contribution from CH_2 carbons of Kristalex™ 5140 can be observed between 30 and 50 ppm. At higher chemical shifts (100–160 ppm), signals from aromatic and alkene carbons were detected. In the spectrum of vSBR_k, it is also possible to observe low intensity signals at about 167 and 87 ppm due to the first-order spinning sidebands of the tertiary aromatic carbons of the resin. In the ^{13}C CP/MAS spectra, recorded with a short contact time of 0.2 ms (Figure 2c,d), signals arising from rigid domains are enhanced, showing broader lines with respect to the DE spectra. In particular, the signals of resin carbons are favored compared to those of SBR, as can be seen from the higher intensity of the spinning sidebands. The isotropic signal and the corresponding sidebands of aromatic tertiary carbons of Kristalex™ 5140 were assigned on the basis of the ^{1}H-^{13}C CP spectrum recorded for the resin under the same experimental conditions (Figure 2e). Interestingly, the observation of spinning sidebands for Kristalex™ 5140 in the spectra of vSBR_k indicates that the resin maintains a rigid character even when blended with the polymer, in agreement with the results from ^{1}H FID analysis.
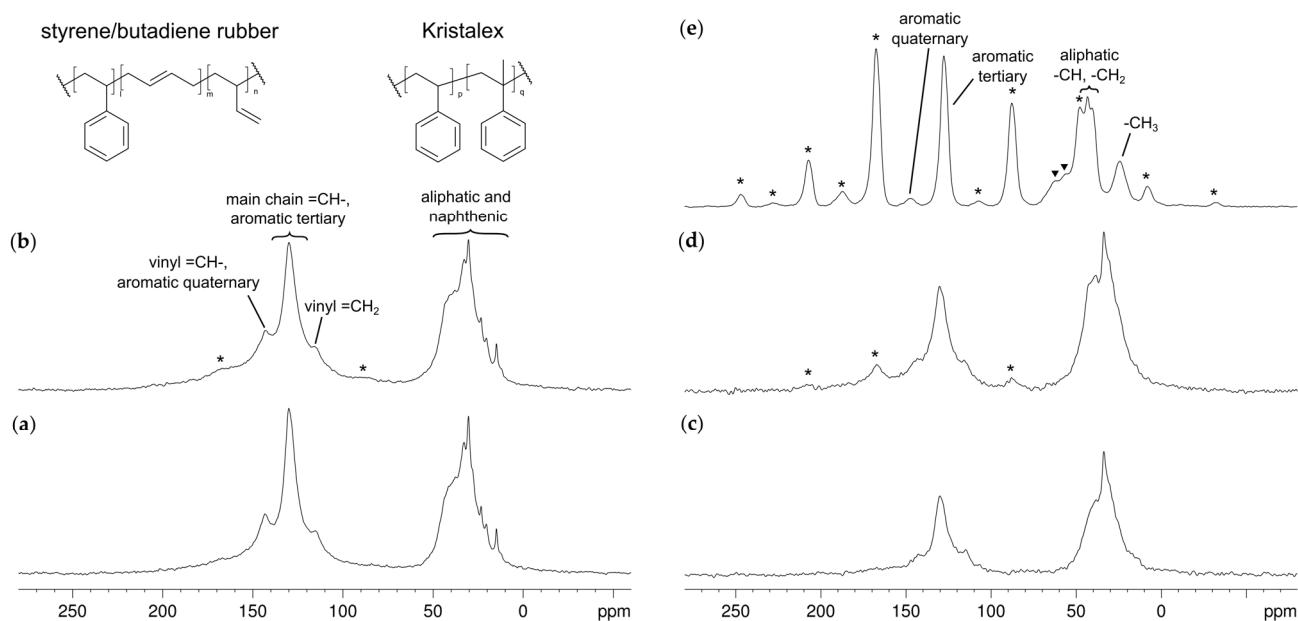
Figure 2. ^{13}C DE/MAS spectra of (**a**) vSBR and (**b**) vSBR_k recorded using a recycle delay of 20 s. ^{1}H-^{13}C CP/MAS spectra of (**c**) vSBR, (**d**) vSBR_k and (**e**) Kristalex™ 5140 recorded using a contact time of 0.2 ms and a recycle delay of 4 s. Spinning sidebands are marked with an asterisk; impurities are marked with a filled triangle. All spectra were recorded using an MAS frequency of 5 kHz.

The CP dynamics was then studied for the tertiary aromatic carbons in pure Kristalex™ 5140 and in vSBR_k and compared with that of aromatic/alkene carbons in vSBR and vSBR_k (see Supplementary Materials). Interestingly, the ^{1}H $T_{1\rho}$ of the aromatic protons of the resin in pure Kristalex™ 5140 (~9 ms) is significantly longer than that measured in both vSBR_k and vSBR (0.6–1 ms) (Table S1). This seems to be ascribable to the proton spin diffusion between resin and polymer domains occurring in vSBR_k and suggests that in this sample the resin is intimately mixed with the polymer. To this regard, further information could be obtained by the low-resolution measurement of ^{1}H T_1: mono-exponential trends for the relaxation curves were obtained for all the samples and ^{1}H T_1 values of 114, 66 and 74 ms were measured for pure Kristalex, vSBR and vSBR_k, respectively. Although these values are quite similar, these results seem to confirm an intimate mixing (on a tens of nm scale) between resin and polymer in vSBR_k.

3.2. Characterization of Dynamics

The dynamic properties of all samples were investigated by means of FC NMR experiments for the measurement of ^{1}H spin–lattice relaxation rates ($R_1 = 1/T_1$) at variable Larmor frequencies, from 0.01 to 35 MHz. In fact, ^{1}H spin–lattice relaxation is driven by the modulation of the ^{1}H-^{1}H dipolar couplings by molecular motions. The dependence of ^{1}H R_1 on frequency (ν or $\omega = 2\pi\nu$), called nuclear magnetic relaxation dispersion (NMRD), can be described by a linear combination of spectral densities, $J(\omega)$, which are the Fourier transform of the autocorrelation functions of motion [43]. For polymers far above T_g, R_1 dispersions are mainly governed by segmental dynamics, that is local motions within the Kuhn segment, activated at the glass transition. Segmental dynamics, also referred to as "glassy" dynamics, is responsible for the so-called α-relaxation. Additional contributions to R_1 dispersions arise from collective motions involving longer and longer chain portions, indicated as polymer dynamics. The contribution to $R_1(\omega)$ arising from segmental dynamics can be well represented using the Cole–Davidson spectral density, while contributions from polymer dynamics result in power law dependences of the type $R_1(\omega) \propto \omega^{-\gamma}$, with different values of the γ exponent depending on the motional regime as defined by the mostly accepted tube–reptation theory [44–46]. Therefore, FC NMR has proven to be an effective technique to characterize the dynamics of polymers far above

glass transition over a broad range of characteristic motion times [47,48]. In particular, it has been successfully applied to obtain information on segmental and polymer dynamics in polymer melts and vulcanized rubbers [49–54]. For this aim, $R_1(\omega)$ data are usually transformed to the susceptibility representation, $\chi''(\omega) = \omega R_1(\omega)$, and $\chi''(\omega\tau_s)$ master curves are built from $\chi''(\omega)$ curves acquired at different temperatures by exploiting the frequency–temperature superposition (FTS) principle [55,56] to determine the values of the correlation time for segmental dynamics, τ_s. At low temperatures, $\chi''(\omega)$ curves show a maximum, and the high-frequency branch of the curves, which mainly arises from the contribution of segmental dynamics ($\chi''_{seg}(\omega)$), can be fitted to Equation (2):

$$\chi''_{seg}(\omega) = \omega K_{CD}[J_{CD}(\omega) + 4J_{CD}(2\omega)] \qquad (2)$$

using the Cole–Davidson spectral density function:

$$J_{CD}(\omega) = \frac{2\sin[\beta_{CD}\arctan(\omega\tau_{CD})]}{\omega[1 + \omega\tau_{CD}]^{\beta_{CD}/2}} \qquad (3)$$

with $0 < \beta_{CD} \leq 1$. Thus, τ_s values can be obtained from τ_{CD} using the relation $\tau_s = \beta_{CD}\tau_{CD}$. At higher temperatures, the $\chi''(\omega)$ curves do not show a maximum, and the frequency axis is scaled until they overlap the curves obtained at lower temperatures to build the master curve. In this case, τ_s can be determined as the frequency scaling factor.

Here, ^{1}H NMRD curves were acquired for all the investigated samples at different temperatures in the 303–393 K range. In Figure 3a, the curves recorded at 303, 333 and 363 K are reported as examples. In Figure S3, the corresponding $\chi''(\omega)$ curves are also shown.
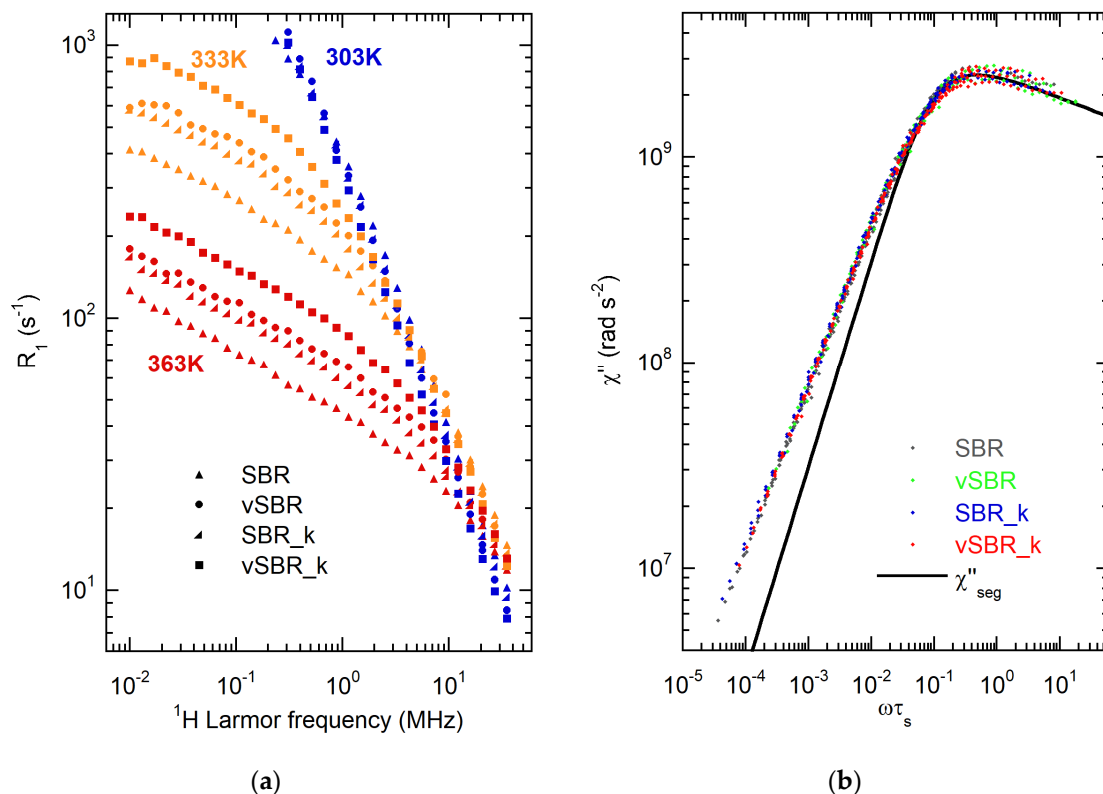

Figure 3. (**a**) ^{1}H NMRD curves for the investigated samples at the indicated temperatures. (**b**) Susceptibility master curves of the indicated samples; the black line represents the contribution of the segmental dynamics to the $\chi''(\omega\tau_s)$ master curve of SBR_k.

For all samples, at low temperatures, R_1 shows a power law dependence on Larmor frequency with $\gamma \cong 1$, suggesting that R_1 relaxation is dominated by segmental dynamics (Regime 0). Correspondingly, the $\chi''(\omega)$ curves display a maximum associated with the

condition $\omega\tau_s \cong 1$, which shifts towards lower frequencies passing from uncured to vulcanized samples. Moreover, SBR_k and vSBR_k show $\chi''(\omega)$ maxima at lower frequencies than the corresponding samples without Kristalex™ 5140. These results indicate a slowdown of segmental dynamics as a consequence of both crosslinking and resin addition, in agreement with the higher T_g values measured by DSC (Table 2). At $T \geq 323$ K, the NMRD curves show two regions with different power law dependences. A region with γ values in the range 0.7–0.8, with γ decreasing by increasing the temperature, was detected at higher frequencies, ascribable to the overlap of Regime 0 with the Rouse regime (Regime I of the tube–reptation model). At lower frequencies, a region with γ of 0.25–0.28 was observed, which is attributable to the Rouse regime. For all samples, R_1 increases with increasing temperature at high frequencies, while it decreases at lower frequencies, with a shift in the crossover point between Regime 0 and Regime I toward lower frequencies, due to the corresponding increase in τ_s.

For each sample, the NMR susceptibility $\chi''(\omega)$ curves obtained at different temperatures were combined together to build $\chi''(\omega\tau_s)$ master curves, under the assumption that the FTS principle holds true, to obtain τ_s values. $\chi''(\omega)$ curves at 303 K were fitted to Equation (2) in order to obtain τ_s. β_{CD} was found to be 0.12, in agreement with the value determined for SBR samples in a previous work [52]. At the remaining temperatures, τ_s values were determined as the frequency scaling factors used to build the master curves. The $\chi''(\omega\tau_s)$ master curves obtained for all samples are shown in Figure 3b, while the values of τ_s as a function of $1000/T$ are reported in Figure 4a. The obtained $\chi''(\omega\tau_s)$ master curves cover a frequency range of six decades and display characteristic shapes that well reflect the different dynamic regimes described above: at a high frequency, the contribution of segmental dynamics is dominant, while polymer dynamics assumes a significant importance for $\omega\tau_s < 0.1$.
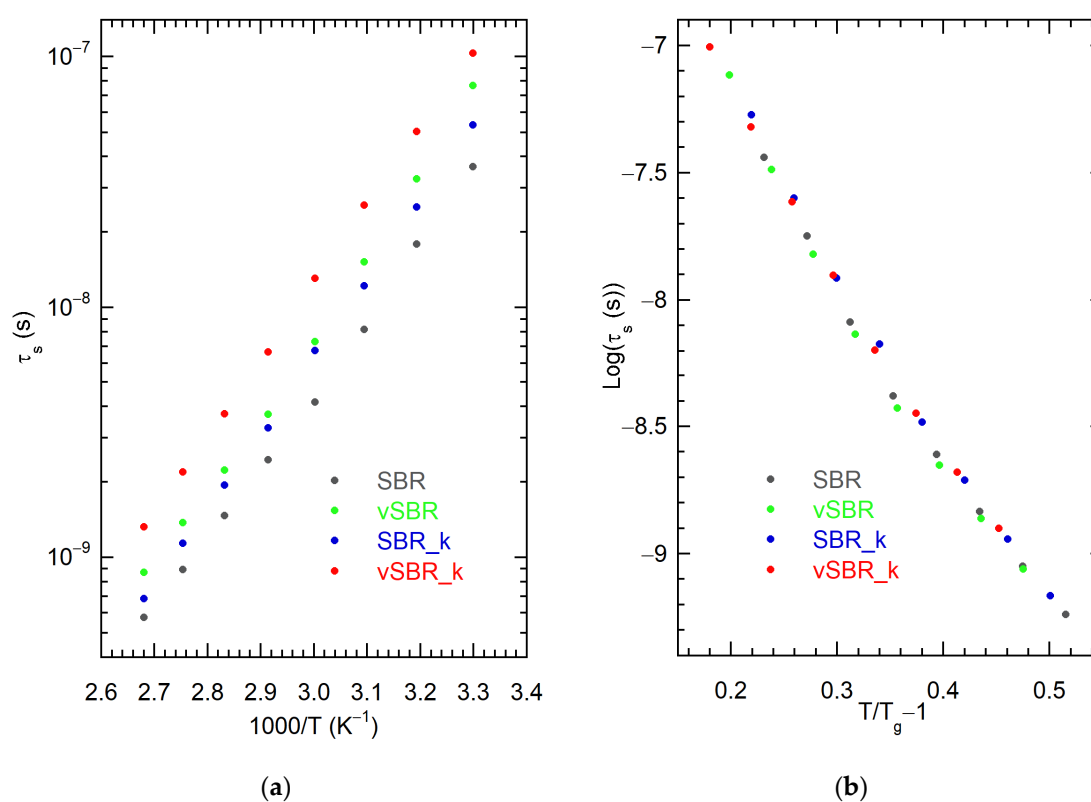

(**a**)　　　　　　　　　　(**b**)

Figure 4. (**a**) Correlation times for segmental dynamics, τ_s, vs. $1000/T$ and (**b**) $\mathrm{Log}\tau_s$ vs. $(T/T_g - 1)$ for the indicated samples. T_g values were determined by DSC measurements (Table 2). Errors on τ_s are lower than 5%.

As expected from the trend of the maxima of the $\chi''(\omega)$ curves, τ_s values are longer in the vulcanized samples (vSBR, vSBR_k) with respect to the uncured ones (SBR, SBR_k), and in samples containing the resin (SBR_k, vSBR_k) with respect to those without it (SBR, vSBR). The increase in τ_s upon vulcanization is ascribable to the formation of crosslinks, which restrict segmental dynamics, also resulting in increased T_g (Table 2). The addition of the resin, although lowering the efficiency of vulcanization, as it was observed when comparing the crosslink density of vSBR and vSBR_k (Table 2), yielded a slowdown of segmental dynamics, paralleled by an increase in T_g. Similar trends in τ_s upon resin addition to rubber matrices were found in investigations of α-relaxation by broadband dielectric spectroscopy [13–15]

For all samples, τ_s values show, as expected, decreasing trends by increasing the temperature (Figure 4a). However, quantitative analyses of these trends in terms of the commonly used Vogel−Fulcher−Tammann (VFT) function to obtain information on polymer fragility is hampered by the limited temperature range investigated. On the other hand, hints on the variation of fragility upon vulcanization or resin addition can be achieved by plotting $Log\tau_s$ as a function of $(T/T_g - 1)$ according to Equation (4):

$$Log\left(\frac{\tau_s(T)}{\tau_0}\right) = \frac{Log^2\left(\frac{\tau_s(T_g)}{\tau_0}\right)}{m\left(\frac{T}{T_g} - 1\right) + Log\left(\frac{\tau_s(T_g)}{\tau_0}\right)} \tag{4}$$

Equation (4) is obtained by recasting the VFT equation [57]. In Equation (4), m is the fragility index, τ_0 is the pre-exponential factor of the VFT equation and the value of τ_s at the glass transition ($\tau_s(T_g)$) is, by definition, a constant (100 s) [58]. If τ_0 and m do not change significantly, all samples are expected to exhibit the same behavior. Indeed, in our case, using T_g values determined by DSC in $(T/T_g - 1)$, a good superposition was observed for the $Log\tau_s$ curves of all the samples (Figure 4b). These results indicate that both crosslinking by vulcanization and resin addition do not significantly affect the polymer fragility index, which yields a measurement of the rapidity with which segmental dynamics slow down upon approaching the glass transition by decreasing the temperature. Unchanged polymer fragility upon vulcanization was also reported for rubbers with low crosslinking degrees [52]. On the other hand, the addition of resin was previously found to increase the fragility index at high resin concentrations [13], suggesting that in our case the amount of resin was too low to show such an effect.

For the vulcanized samples, the dynamics at low frequency was further investigated by analyzing ^{1}H spin–lattice relaxation in the rotating frame ($T_{1\rho}$). Although an estimate of ^{1}H $T_{1\rho}$ was already obtained by analyzing the CP dynamics, ^{1}H $T_{1\rho}$ data were more accurately measured at a spinlock field ($\omega_1/2\pi$) of 46 kHz by means of a dedicated experiment with direct ^{1}H detection. At all the investigated temperatures (from 303 to 343 K), the relaxation curves can be well reproduced by the combination of two exponential functions $I(t) = I(0)\left(W_a e^{-\frac{t}{T_{1\rho,a}}} + W_b e^{-\frac{t}{T_{1\rho,b}}}\right)$, with $W_a \cong$ 40–90%, $T_{1\rho,a} \cong$ 0.6–2.3 ms, $W_b \cong$ 10–60% and $T_{1\rho,b} \cong$ 5–11 ms, which is very similar for vSBR and vSBR_k, as shown in Table S2. The effect of spin diffusion, which tends to average out differences between intrinsic relaxation times, makes a physical interpretation of the individual $T_{1\rho}$ components very difficult. Nevertheless, dynamic information could be obtained by looking at the population weighted rate average $R_{1\rho}^{PWRA} = \frac{W_a}{T_{1\rho,a}} + \frac{W_b}{T_{1\rho,b}}$, which is not affected by spin diffusion [29] (Table S3). As shown in Figure 5, ^{1}H $R_{1\rho}^{PWRA}$ decreases by increasing the temperature for both vSBR and vSBR_k, indicating the presence of dynamic processes in the fast motion regime. In agreement with R_1 measurements, higher $R_{1\rho}^{PWRA}$ values were measured for vSBR_k, which shows a higher T_g, indicating a slowdown of dynamics induced by the presence of the resin. In order to better understand the origin of $R_{1\rho}^{PWRA}$ relaxation, the

contribution of segmental dynamics ($R_{1\rho}^{seg}$) at different temperatures was calculated from Equation (5):

$$R_{1\rho}^{seg}(\omega, \omega_1) = \frac{K_{CD}}{2}[5J_{CD}(\omega) + 2J_{CD}(\omega) + 3J_{CD}(2\omega_1)] \qquad (5)$$

The values of τ_s obtained from the analysis of ^{1}H NMRD curves and reported in Figure 4 were used for the calculation. As we can see, $R_{1\rho}^{seg}$ shows a decreasing trend with increasing temperature, but it accounts for only a fraction, ranging from about 52% at 303 K to 14% at 343 K, of the experimental ^{1}H $R_{1\rho}^{PWRA}$. This confirms the increasing contribution of collective polymer dynamics in the kHz frequency range as the temperature increases. The contribution of polymer dynamics was estimated as the difference $R_{1\rho}^{pol} = R_{1\rho}^{PWRA} - R_{1\rho}^{seg}$ (Figure 5, Table S3), under the assumption of statistical independence and time-scale separation between segmental and polymer dynamics. $R_{1\rho}^{pol}$ increases by decreasing the temperature, approaching a maximum at 303–313 K that corresponds to the condition $\omega_1\tau_{pol} \cong 1$. These results suggest the presence of Rouse motions with characteristic correlation times (τ_{pol}) on the order of tens of μs in the investigated temperature range.
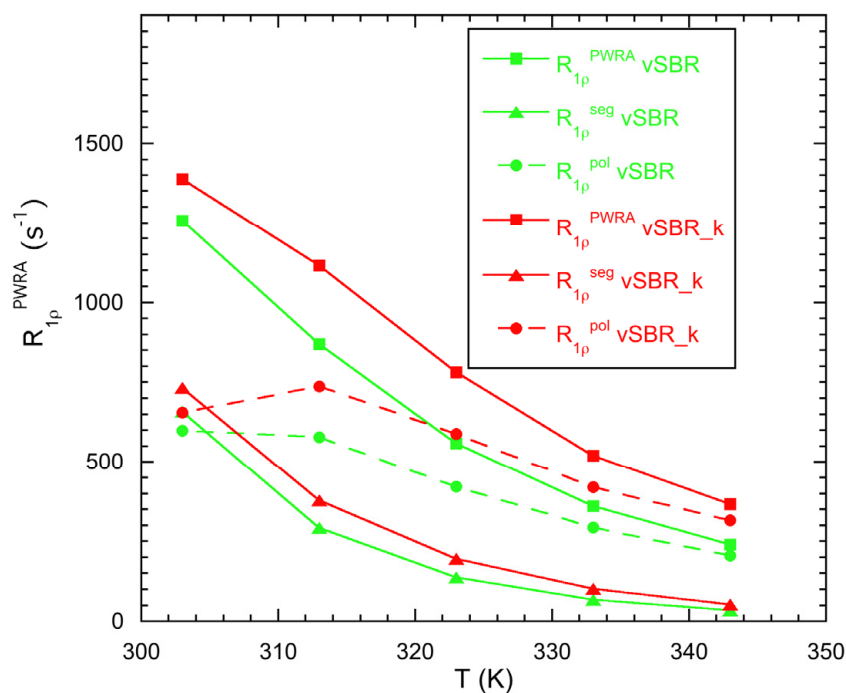
Figure 5. ^{1}H $R_{1\rho}^{PWRA}$ (experimental), $R_{1\rho}^{seg}$ (calculated) and $R_{1\rho}^{pol}$ (calculated) vs. temperature for the indicated samples. The lines are plotted to guide the eye.

4. Conclusions

In this work, the effects of the tackifying resin Kristalex™ 5140 on the structural and dynamic properties of SBR compounds of interest to the tire industry were investigated through a combination of high-resolution and TD SSNMR techniques. To this end, uncured and cured SBR compounds, either in the absence or presence of 15 phr of resin, as well as a pure Kristalex™ 5140 sample, were studied, and the obtained results were discussed in comparison with T_g and crosslink density data.

From the "macroscopic" point of view, an increase in T_g and a slight decrease in crosslink density were observed as a consequence of resin addition. From the "microscopic" point of view, the resin was found to be intimately mixed with the polymer in the rubber matrix, while maintaining its rigid character. Moreover, the resin induced a slowdown of segmental dynamics of the polymer in both uncured and cured samples, while it did

not affect the polymer fragility and the spectrum of collective polymer motions in the Rouse regime.

In conclusion, the obtained results showed for the first time that SSNMR can provide very useful information on the degree of mixing and interaction between resin and polymer in rubber compounds. This information could help the comprehension of the molecular origin of the observed macroscopic and mechanical properties, which is fundamental to drive research towards formulations with improved and optimized performances.

References

1. Rodgers, B.; Waddell, W. Chapter 9—The Science of Rubber Compounding. In *The Science and Technology of Rubber*, 4th ed.; Mark, J.E., Erman, B., Roland, C.M., Eds.; Academic Press: Boston, MA, USA, 2013; pp. 417–471.
2. Stuck, B. Tackifying, Curing, and Reinforcing Resins. In *Rubber Technology*; Carl Hanser Verlag GmbH & Co. KG: München, Germany, 2020; pp. 641–651.
3. Powers, P.O. Resins Used in Rubber. *Rubber Chem. Technol.* **1963**, *36*, 1542–1570. [CrossRef]
4. Kim, S.W.; Lee, G.H.; Heo, G.S. Identification of Tackifying Resins and Reinforcing Resins in Cured Rubber. *Rubber Chem. Technol.* **1999**, *72*, 181–198. [CrossRef]
5. Aubrey, D.W. The Nature and Action of Tackifier Resins. *Rubber Chem. Technol.* **1988**, *61*, 448–469. [CrossRef]
6. Vleugels, N.; Pille-Wolf, W.; Dierkes, W.K.; Noordermeer, J.W.M. Understanding the Influence of Oligomeric Resins on Traction and Rolling Resistance of Silica-Reinforced Tire Treads. *Rubber Chem. Technol.* **2015**, *88*, 65–79. [CrossRef]

7. Indriasari; Noordermeer, J.; Dierkes, W. Incorporation of Oligomeric Hydrocarbon Resins for Improving the Properties of Aircraft Tire Retreads. *Appl. Sci.* **2021**, *11*, 9834. [CrossRef]

8. Class, J.B.; Chu, S.G. The Viscoelastic Properties of Rubber–Resin Blends. I. The Effect of Resin Structure. *J. Appl. Polym. Sci.* **1985**, *30*, 805–814. [CrossRef]

9. Class, J.B.; Chu, S.G. The Viscoelastic Properties of Rubber–Resin Blends. II. The Effect of Resin Molecular Weight. *J. Appl. Polym. Sci.* **1985**, *30*, 815–824. [CrossRef]

10. Class, J.B.; Chu, S.G. The Viscoelastic Properties of Rubber–Resin Blends. III. The Effect of Resin Concentration. *J. Appl. Polym. Sci.* **1985**, *30*, 825–842. [CrossRef]

11. L'Heveder, S.; Sportelli, F.; Isitman, N.A. Investigation of Solubility in Plasticised Rubber Systems for Tire Applications. *Plast. Rubber Compos.* **2016**, *45*, 319–325. [CrossRef]

12. Lindemann, N.; Finger, S.; Karimi-Varzaneh, H.A.; Lacayo-Pineda, J. Rigidity of Plasticizers and Their Miscibility in Silica-Filled Polybutadiene Rubber by Broadband Dielectric Spectroscopy. *J. Appl. Polym. Sci.* **2022**, *139*, 52215. [CrossRef]

13. Lindemann, N.; Schawe, J.E.K.; Lacayo-Pineda, J. Kinetics of the Glass Transition of Silica-Filled Styrene–Butadiene Rubber: The Effect of Resins. *Polymers* **2022**, *14*, 2626. [CrossRef]

14. Liang, J.; Chang, S.; Feng, N. Effect of C5 Petroleum Resin Content on Damping Behavior, Morphology, and Mechanical Properties of BIIR/BR Vulcanizates. *J. Appl. Polym. Sci.* **2013**, *130*, 510–515. [CrossRef]

15. Yin, C.; Zhao, X.; Zhu, J.; Hu, H.; Song, M.; Wu, S. Experimental and Molecular Dynamics Simulation Study on the Damping Mechanism of C5 Petroleum Resin/Chlorinated Butyl Rubber Composites. *J. Mater. Sci.* **2019**, *54*, 3960–3974. [CrossRef]

16. Guo, Y.; Liu, J.; Lu, Y.; Dong, D.; Wang, W.; Zhang, L. A Combined Molecular Dynamics Simulation and Experimental Method to Study the Compatibility between Elastomers and Resins. *RSC Adv.* **2018**, *8*, 14401–14413. [CrossRef]

17. Dae Han, C.; Kim, J.; Man Baek, D.; Gun Chu, S. Viscoelastic Behavior, Order-Disorder Transition, and Phase Equilibria in Mixtures of a Block Copolymer and an Endblock-Associating Resin. *J. Polym. Sci. Part B Polym. Phys.* **1990**, *28*, 315–341. [CrossRef]

18. Harper, M.; Tardiff, J.; Haakenson, D.; Joandrea, M.; Knych, M. Tire Tread Performance Modification Utilizing Polymeric Additives. *SAE Int. J. Veh. Dyn. Stab. NVH* **2017**, *2*, 179–189. [CrossRef]

19. Hu, X.; Zhang, R.; Wemyss, A.M.; Du, A.; Bao, X.; Geng, X.; Wan, C. Damping and Electromechanical Behavior of Ionic-Modified Brominated Poly(Isobutylene-*Co*-Isoprene) Rubber Containing Petroleum Resin C5. *Ind. Eng. Chem. Res.* **2022**, *61*, 3063–3074. [CrossRef]

20. Ye, N.; Wu, Z.; Wu, X.; Lu, Y.; Zhang, L. Performance Enhancement of Polymerized, Functionalized Solution Styrene–Butadiene Rubber Composites Using Oligomeric Resin towards Extremely Safe and Energy-Saving Tires. *Polymers* **2022**, *14*, 2928. [CrossRef]

21. Wu, C.; Wu, G.; Wu, C. Dynamic Mechanical Properties in Blends of Poly(Styrene-b-Isoprene-b-Styrene) with Aromatic Hydrocarbon Resin. *J. Appl. Polym. Sci.* **2006**, *102*, 4157–4164. [CrossRef]

22. Schmidt-Rohr, K.; Spiess, H.W. *Multidimensional Solid-State NMR and Polymers*; Elsevier: Amsterdam, The Netherlands, 1994.

23. Saalwächter, K.; Spiess, H.W. Solid-State NMR of Polymers. In *Polymer Science: A Comprehensive Reference*; Matyjaszewski, K., Möller, M., Eds.; Elsevier: Amsterdam, The Netherlands, 2012; pp. 185–219.

24. Saalwächter, K.; Reichert, D. Polymer Applications of NMR. *Encycl. Spectrosc. Spectrom.* **2016**, 695–708. [CrossRef]

25. Zhang, R.; Miyoshi, T.; Sun, P. *NMR Methods for Characterization of Synthetic and Natural Polymers*; Royal Society of Chemistry: London, UK, 2019.

26. Müller, K.; Geppi, M. Chapter 8—Application of SSNMR to Selected Classes of Systems. In *Solid State NMR: Principles, Methods and Applications*; Wiley-VCH: Weinheim, Germany, 2021; pp. 447–530.

27. Saalwächter, K. Microstructure and Molecular Dynamics of Elastomers as Studied By Advanced Low-Resolution Nuclear Magnetic Resonance Methods. *Rubber Chem. Technol.* **2012**, *85*, 350–386. [CrossRef]

28. Besghini, D.; Mauri, M.; Simonutti, R. Time Domain NMR in Polymer Science: From the Laboratory to the Industry. *Appl. Sci.* **2019**, *9*, 1801. [CrossRef]

29. Geppi, M.; Harris, R.K.; Kenwright, A.M.; Say, B.J. A Method for Analysing Proton NMR Relaxation Data from Motionally Heterogeneous Polymer Systems. *Solid State Nucl. Magn. Reson.* **1998**, *12*, 15–20. [CrossRef] [PubMed]

30. Forte, C.; Geppi, M.; Malvaldi, M.; Mattoli, V. Dynamics of an Amorphous Polymer by an Improved NMR Approach Based on the Simultaneous Analysis of ^{1}H and ^{13}C Relaxation Times. *J. Phys. Chem. B* **2004**, *108*, 10832–10837. [CrossRef]

31. Martini, F.; Borsacchi, S.; Spera, S.; Carbonera, C.; Cominetti, A.; Geppi, M. P3HT/PCBM Photoactive Materials for Solar Cells: Morphology and Dynamics by Means of Solid-State NMR. *J. Phys. Chem. C* **2013**, *117*, 131–139. [CrossRef]

32. TECHNICAL DATA SHEET Kristalex™ 5140 Hydrocarbon Resin. Available online: www.synthomer.com/Media/tds/Kristalex%205140%20Hydrocarbon%20Resin.pdf (accessed on 23 January 2023).

33. Saville, B.; Watson, A.A. Structural Characterization of Sulfur-Vulcanized Rubber Networks. *Rubber Chem. Technol.* **1967**, *40*, 100–148. [CrossRef]

34. *Mathematica*, Version 12; Wolfram Research, Inc.: Champaign, IL, USA, 2010.

35. Maus, A.; Hertlein, C.; Saalwächter, K. A Robust Proton NMR Method to Investigate Hard/Soft Ratios, Crystallinity, and Component Mobility in Polymers. *Macromol. Chem. Phys.* **2006**, *207*, 1150–1158. [CrossRef]

36. Papon, A.; Saalwächter, K.; Schäler, K.; Guy, L.; Lequeux, F.; Montes, H. Low-Field NMR Investigations of Nanocomposites: Polymer Dynamics and Network Effects. *Macromolecules* **2011**, *44*, 913–922. [CrossRef]

37. Räntzsch, V.; Haas, M.; Özen, M.B.; Ratzsch, K.F.; Riazi, K.; Kauffmann-Weiss, S.; Palacios, J.K.; Müller, A.J.; Vittorias, I.; Guthausen, G.; et al. Polymer Crystallinity and Crystallization Kinetics via Benchtop ^{1}H NMR Relaxometry: Revisited Method, Data Analysis, and Experiments on Common Polymers. *Polymer* **2018**, *145*, 162–173. [CrossRef]

38. Borsacchi, S.; Sudhakaran, U.P.; Calucci, L.; Martini, F.; Carignani, E.; Messori, M.; Geppi, M. Rubber-Filler Interactions in Polyisoprene Filled with in Situ Generated Silica: A Solid State NMR Study. *Polymers* **2018**, *10*, 822. [CrossRef]

39. Nardelli, F.; Martini, F.; Lee, J.; Lluvears-Tenorio, A.; La Nasa, J.; Duce, C.; Ormsby, B.; Geppi, M.; Bonaduce, I. The Stability of Paintings and the Molecular Structure of the Oil Paint Polymeric Network. *Sci. Rep.* **2021**, *11*, 1–13. [CrossRef]

40. Perez, M.G.; Lima, A.P.; Moraes, T.B.; Chaves, E.G.; Ruiz, N.M.D.S.; dos Santos Teixeira, S.C.; Honorato, H.D.A.; de Menezes, S.M.C.; deAzevedo, E.R. ^{1}H Time Domain NMR to Probe Microstructural and Mobility Changes in Polyamide 11 Exposed to H_2S Scavengers. What Type of Information Can Be Assessed? *Polym. Degrad. Stab.* **2022**, *202*, 110001. [CrossRef]

41. Schäler, K.; Roos, M.; Micke, P.; Golitsyn, Y.; Seidlitz, A.; Thurn-Albrecht, T.; Schneider, H.; Hempel, G.; Saalwächter, K. Basic Principles of Static Proton Low-Resolution Spin Diffusion NMR in Nanophase-Separated Materials with Mobility Contrast. *Solid State Nucl. Magn. Reson.* **2015**, *72*, 50–63. [CrossRef]

42. Hansen, E.W.; Kristiansen, P.E.; Pedersen, B. Crystallinity of Polyethylene Derived from Solid-State Proton NMR Free Induction Decay. *J. Phys. Chem. B* **1998**, *102*, 5444–5450. [CrossRef]

43. Abragam, A. *The Principles of Nuclear Magnetism*; Clarendon Press: Oxford, UK; London, UK, 1961.

44. Doi, M.; Edwards, S.F. *The Theory of Polymer Dynamics*; Science Publication: Oxford, UK; London, UK, 1986.

45. de Gennes, P.G. Reptation of a Polymer Chain in the Presence of Fixed Obstacles. *J. Chem. Phys.* **1971**, *55*, 572–579. [CrossRef]

46. Rouse, P.E. A Theory of the Linear Viscoelastic Properties of Dilute Solutions of Coiling Polymers. *J. Chem. Phys.* **1953**, *21*, 1272–1280. [CrossRef]

47. Kimmich, R.; Fatkullin, N. Polymer Chain Dynamics and NMR. *Adv. Polym. Sci.* **2004**, *170*, 1–113. [CrossRef]

48. Stapf, S.; Lozovoi, A. Chapter 13. Field-Cycling Relaxometry of Polymers. In *Field-Cycling NMR Relaxometry*; Kimmich, R., Ed.; The Royal Society of Chemistry: Cambridge, UK, 2018; pp. 322–357.

49. Kariyo, S.; Stapf, S. Influence of Cross-Link Density and Deformation on the NMR Relaxation Dispersion of Natural Rubber. *Macromolecules* **2002**, *35*, 9253–9255. [CrossRef]

50. Kariyo, S.; Stapf, S. NMR Relaxation Dispersion of Vulcanized Natural Rubber. *Solid State Nucl. Magn. Reson.* **2004**, *25*, 64–71. [CrossRef]

51. Kariyo, S.; Stapf, S. Restricted Molecular Dynamics of Polymer Chains by Means of NMR Field Cycling Relaxometry. *Macromol. Chem. Phys.* **2005**, *206*, 1300–1310. [CrossRef]

52. Martini, F.; Carignani, E.; Nardelli, F.; Rossi, E.; Borsacchi, S.; Cettolin, M.; Susanna, A.; Geppi, M.; Calucci, L. Glassy and Polymer Dynamics of Elastomers by ^{1}H Field-Cycling NMR Relaxometry: Effects of Cross-Linking. *Macromolecules* **2020**, *53*, 10028–10039. [CrossRef] [PubMed]

53. Nardelli, F.; Martini, F.; Carignani, E.; Rossi, E.; Borsacchi, S.; Cettolin, M.; Susanna, A.; Arimondi, M.; Giannini, L.; Geppi, M.; et al. Glassy and Polymer Dynamics of Elastomers by ^{1}H-Field-Cycling NMR Relaxometry: Effects of Fillers. *J. Phys. Chem. B* **2021**, *125*, 4546–4554. [CrossRef] [PubMed]

54. Nardelli, F.; Calucci, L.; Carignani, E.; Borsacchi, S.; Cettolin, M.; Arimondi, M.; Giannini, L.; Geppi, M.; Martini, F. Influence of Sulfur-Curing Conditions on the Dynamics and Crosslinking of Rubber Networks: A Time-Domain NMR Study. *Polymers* **2022**, *14*, 767. [CrossRef] [PubMed]

55. Ferry, J.D. *Viscoelastic Properties of Polymers*, 3rd ed.; John Wiley & Sons: New York, NY, USA, 1980.

56. Ding, Y.; Sokolov, A.P. Breakdown of Time−Temperature Superposition Principle and Universality of Chain Dynamics in Polymers. *Macromolecules* **2006**, *39*, 3322–3326. [CrossRef]

57. Blochowicz, T.; Gainaru, C.; Medick, P.; Tschirwitz, C.; Rössler, E.A. The Dynamic Susceptibility in Glass Forming Molecular Liquids: The Search for Universal Relaxation Patterns II. *J. Chem. Phys.* **2006**, *124*, 134503. [CrossRef]

58. Kremer, F.; Schönhals, A. *Broadband Dielectric Spectroscopy*; Kremer, F., Schönhals, A., Eds.; Springer: Berlin/Heidelberg, Germany; New York, NY, USA, 2003.